A challenge in biosensors: Is it better to measure a photon or an electron for ultrasensitive detection?

A CHALLENGE IN BIOSENSORS: IS IT BETTER TO MEASURE A PHOTON OR AN ELECTRON FOR ULTRASENSITIVE DETECTION?

Aldo Roda*[1,2], Fabiana Arduini[3], Mara Mirasoli[1,2], Martina Zangheri[1], Laura Fabiani[3], Noemi Colozza[3], Elisa Marchegiani[1], Patrizia Simoni[4], Danila Moscone*[3]

[1]Department of Chemistry "Giacomo Ciamician", Alma Mater Studiorum – University of Bologna, Via Selmi 2, 40126 Bologna, Italy

[2] Biostructures and Biosystems National Institute (INBB), Viale delle Medaglie d'Oro 305, 00136 Rome, Italy

[3] Department of Chemical Science and Technologies, University of Rome Tor Vergata, Via della Ricerca Scientifica 1, 00133 Rome, Italy

[4]Department of Medical and Surgical Sciences, Alma Mater Studiorum – University of Bologna, Via Massarenti 9, 40138 Bologna, Italy

Corresponding authors:

Aldo Roda

Department of Chemistry "Giacomo Ciamician"

Alma Mater Studiorum – University of Bologna

Via Selmi 2, 40126 Bologna, Italy

aldo.roda@unibo.it

Danila Moscone

Department of Chemical Science and Technologies

University of Rome Tor Vergata

Via della Ricerca Scientifica 1, 00133 Rome, Italy

danila.moscone@uniroma2.it

ABSTRACT

Biosensor development exploiting various transduction principles is characterized by a strong competition to reach high detectability, portability and robustness. Nevertheless, a literature-based comparison is not possible, as different conditions are employed in each paper.

Herein, we aim at evaluating which measurement, photons or electrons, yields better biosensor performance. Upon outlining an update in recent achievements to boost analytical performance, amperometry and chemiluminescence (CL)-based biosensors are directly compared employing the same biospecific reagents and analytical formats. Horseradish peroxidase (HRP) and hydrogen peroxide concentrations were directly measured, while glucose and mouse IgG were detected employing an enzyme paper-based biosensor and an immunosensor, respectively.

Detectability was down to picomoles of hydrogen peroxide (4 for CL and 210 pmol for amperometry) and zeptomoles of HRP (45 for CL and 20 zmol for amperometry); IgG was detected down to 12 fM (CL) and 120 fM (amperometry), while glucose down to 17 μM (CL) and 40 μM (amperometry).

Results showed that amperometric and CL biosensors offered similar detectability and analytical performance, with some peculiarities that suggest complementary application fields. As they generally provided slightly higher detectability and wider dynamic ranges, CL-based biosensors appear more suitable for point-of-care testing of clinical biomarkers, where detectability is crucial. Nevertheless, as high detectability in CL biosensors usually requires longer acquisition times, their rapidity will allocate electrochemical biosensors in real-time monitoring and wearable biosensors.

The analytical challenge demonstrated that these biosensors have competitive and similar performance, and between photons and electrons the competition is still open.

1. INTRODUCTION

Nowadays basic research in biosensors is oriented to achieve ultrasensitive detection combined with fast response time, cost-effectiveness, and portability. The WHO has established that an an effective diagnostic test shall fulfil the ASSURED criteria, where ASSURED means: **A**ffordable (by those at risk of infection), **S**ensitive (low false-negatives), **S**pecific (few false-positives), **U**ser-friendly (simple to perform and requiring minimal training), **R**apid (to give useful information at first visit) and **R**obust (do not require refrigerated storage), **E**quipment-free, **D**elivered to those who need it. In the attempt to reach these goals, many incredible advances in the field of biosensors have been achieved over the past decade, underpinned by a variety of solutions to boost sensitivity and selectivity.

From the commercial and diagnostic point of view, two fantastic successes have boosted the market penetration of biosensors, paving the way for point-of-care testing (POCT). In 1980, miniaturized electrochemical glucose biosensors, such as Glucopen or similar devices, opened a new era in the diabetes management, enabling for the first time the patient to autonomously measure at home his glucose in blood, with high impact on his quality of life and on cost in charge of the National Health Service. Another biosensor playing a leading role in POCT market is the lateral flow immunoassay (LFIA)-based pregnancy test, first released by Clearblue in 1988, which employs nanoparticles for a color-based visual readout. While for glucose detection high assay sensitivity was not the main issue, being glucose present in blood at millimolar levels, high detectability for urinary human chorionic gonadotropin was fundamental to early establish pregnancy (Campbell et al., 1987).

In the subsequent decades, there has been an explosion of biosensing related technologies, taking advantages of new (nano)materials, advanced protein chemistry and molecular biology, protein immobilization procedures and modern approaches to signal transduction, associated with any kind of electronics and microfluidics to assist the biosensor format.

A large number of papers have been published in the last twenty years, exploiting different transduction principles, from electrochemical (such as conductometric, voltammetric, potentiometric, amperometric, and impedimetric detection), through optical (including absorbance/reflectometry, photoluminescence, bio-chemiluminescence (BL/CL), and thermochemiluminescence), hybrid photon-electron systems (such as electrogenerated chemiluminescence (ECL) and photoelectrochemistry), up to label-free formats (including for example surface plasmon resonance principle, magnetic, calorimetric, acoustic, and mass sensitive detection principles).

Surprisingly, these very new exciting biosensor principles just represent elegant proof of concept approaches, while they are not able to achieve a wide diffusion in the market: few commercially

biosensors are so far available in the market or limited to small-scale distribution by start-up high-tech companies.

The main barriers are not only related to the biosensor *per se*, but mainly to problems in managing quality control of the data, robustness of the devices and all the related certified procedures requested in the clinical chemistry field.

We are in a sort of stagnant situation: many small size enterprises already developed new biosensors but with problems to enter in the medical market, thus hampering the urgent need of diagnosis of many pathologies requiring the sub-picomolar detection of specific biomarkers and the therapeutic monitoring of pharmacological therapies, particularly in the era of precision medicine. This is the emerging field that should stimulate new commercial opportunities for the near future of biosensing technologies already established and optimized, but still orphan.

If we enter in more details in the transduction technologies, electrochemistry dominated in the early years, and the biosensors world was often identified with the electrochemical ones. Moreover, this principle is still the most used in basic and applied research. In the research field second to electrochemical biosensors are those based on optical/luminescence transduction and particularly on chemical luminescence including ECL and CL which potentially combine high detectability with instrumental simplicity and low cost.

The competition among the different transducing principles is very strong in terms of detectability and analytical format, and the different claims reported by the authors do not allow understanding which transduction technologies offer the best potential analytical performance to achieve the highest detectability combined with device simplicity/robustness often requested for new generation biomarker detection assays. Indeed, the intercomparison between different detection principles described in the literature is often affected by differences in the assay format regarding the molecular recognition elements (such as antibody affinity and specificity, enzyme kinetics and catalysis) and assay conditions involving biomolecules immobilization, materials, microfluidic-based formats, etc.

To achieve a realistic and accurate evaluation of the potentiality of electrochemistry and CL (i.e., is it better to “measure a photon or an electron”?), we engaged a collaboration between two research groups, well-recognized experts respectively in electrochemistry and CL-based biosensing. With this aim, biosensors were built up by the two groups in the same analytical format, sharing the same biospecific reagents and protocols. For a wide range and accurate comparison, the challenge was carried out using some biosensor formats widely employed in analytical chemistry from enzymatic to immunological based biosensors.

Horseradish peroxidase (HRP) activity and hydrogen peroxide concentration were measured, being these two molecules used in many coupled enzymatic reactions, and the enzyme often used as a label for affinity binding biosensors.

Glucose was also included in the comparative study, since the only well-established widely commercially available biosensor is the electrochemistry-based one for glucose detection in blood; however, paper-based sensors were utilized, in order to realize new sustainable devices.

Finally, we set up a model sandwich-type immunoassay for rabbit immunoglobulin G (IgG) detection using a specific antibody immobilized on magnetic beads and a secondary HRP-labeled antibody. Each assay was evaluated employing two biosensor device apparatuses: a bench-top instrumentation and a portable miniaturized format.

The obtained results should allow to accurately establish the "winner transduction technology" between the two competitors, which provides the lowest detection limit and highest sensitivity and dynamic range combined with simplicity and amenability for miniaturization and short analysis time.

A suggested allocation of the two principle in different complementary application areas according to their analytical performance will be also reported and discussed.

The final goal was to define the potentiality of the two approaches, offering a useful tool to the scientific community for driving the choice in selecting a most suitable biosensor format for the introduction in the market for a given specific need.

2. AN UPDATE ON FUNDAMENTALS OF ANALYTICAL CHEMILUMINESCENCE AND ELECTROCHEMISTRY

2.1 Fundamental update in analytical chemiluminescence

Chemiluminescence (CL) is the light emission generated by a chemical reaction, in which a singlet chemi-excited (intermediate) product emits a photon (or undergoes energy transfer to a fluorescent acceptor in indirect CL) while decaying to the electronic ground state via S_1-to-S_0 fluorescence decay. Since the first luminol-based CL system was reported (Albrecht 1928), several CL substrates, such as lucigenin, lophine, acridinium/acridan esters, peroxyoxalates, and 1,2-dioxetanes, have been proposed and employed for developing ultrasensitive bioassays. Many known CL systems rely on oxidation-dependent mechanisms, in which a four-membered ring peroxide intermediate (1,2-dioxetane or 1,2-dioxetanone) is formed. These are intrinsically unstable strained heterocyclic compounds bearing the relatively weak O–O bond, which decomposition is exergonic enough to produce carbonyl compounds in the electronic singlet excited state. In other CL systems, first introduced by Schaap in 1987, light emission is chemically- or enzymatically triggered by removal of a phenol-protecting group from a

stable adamantylene-dioxetane derivative. The resulting phenolate decomposes via an intramolecular chemically initiated electron exchange luminescence (CIEEL) with photon emission (Shaap et al., 1987).

Chemiluminescence-based biosensors can also rely on the CL resonance energy transfer (CRET) principle, which involves a non-radiative (dipole-dipole) energy transfer occurring between a CL donor and an energy acceptor (either a fluorophore or a quencher). As this phenomenon only occurs when donor and acceptor are in close proximity (< 10 nm), it provides a powerful tool for the sensitive detection of molecular binding events, similarly to the more common FRET phenomenon.

Compared with photoluminescence, probably the most diffused luminescence-based detection approach, CL share the same S_1-S_0 radiative decay i.e. fluorescence, but generally yields much weaker signals and therefore it requires sensitive light detectors, such as photomultiplier tubes (PMT) or cooled back-illuminated charge-coupled device (CCD) cameras. Nevertheless, CL is characterized by a higher signal/noise ratio, being the background only due to the detector thermal and electronic noise. Indeed, the background phenomena affecting photoluminescence, such as excitation of matrix components or scattering of excitation light, are absent in CL detection.

Recently, various detectors characterized by an adequate sensitivity combined with portability have been proposed, thus solving the main limitation of the relatively weak CL signal and leading to the development of ultrasensitive POCT assays. For example, BL/CL biosensors were designed exploiting new generation of (thermally cooled) back illuminated (BI) CCD (Mirasoli et al., 2018) and smartphone BI-CMOS camera (Zangheri et al., 2015) or thin film photosensors, such as single photon avalanche photodiodes (Iinuma et al., 2016) or amorphous silicon (a-Si:H) photosensors (Zangheri et al., 2016).

In addition to the fact that CL-based detection, differently from photoluminescence, cannot rely on a signal increase obtained by increasing the intensity of the photoexcitation source, the weakness of the CL emissions is due to the low CL quantum yields (Φ_{CL}). For example, the oxidation of luminol, one of the most established CL reactions, gives rise a flash-type emission and displays under optimal conditions a Φ_{CL} of about 1% or less in aqueous solutions. On the contrary, in the case of natural CL, i.e. bioluminescence of the well know luciferase /luciferin system, the Φ_{BL} is higher, reaching almost 50% in optimized condition. The luminol CL reaction mechanism involves the reaction of molecular oxygen with the enol-form of luminol anion; the latter is oxidized to a cyclic peroxide which decomposes to yield 3-aminophthalate (3-amino-1,2-benzenedicarboxylic acid) in an excited state, along with a nitrogen molecule. Although the spontaneous oxidation of luminol in aqueous solution is very slow, it can be catalyzed by peroxidase enzymes, such as HRP, or other one-electron oxidants, such as metals, free radicals and a variety of nanomaterials.

Due to the intrinsic advantages of CL detection in biosensing, continuous work is performed to overcome the poor efficiency of CL reactions and to produce new CL compounds with improved characteristics.

Because peroxidases are poor catalysts in luminol oxidation, enhancers are added to the substrate mixture to increase light output and extend the kinetics of the reaction to a glow-type emission. The enhancer acts as a redox mediator that exchanges electrons between the peroxidase enzyme and luminol. Various molecules have been employed, such as substituted phenols, substituted boronic acids, indophenols, and N-alkyl phenothiazine derivatives. The ability of the enhancer to increase the intensity of light emission is due to two effects: increased rate of HRP turnover and reversible electron transfer between enhancer radicals and luminol. In addition to these species (primary enhancers), co-enhancers (or secondary enhancers) can significantly boost the light output by synergistic effect, probably by facilitating the action of the primary enhancer as electron transfer mediator (Sakharov and Vdovenko 2013). Currently the most effective enhancer/co-enhancer system is 3-(10'-phenothiazinyl)propane-1-sulfonate (SPTZ) in the presence of 4-morpholinopyridine (MORP) developed by our group, that pushed the limit of detection for HRP down to few amol (Marzocchi et al., 2008). In recent years, some chemical indicators, such as bromophenol red or bromophenol blue, have demonstrated enhancing properties towards the HRP-luminol-H_2O_2 reaction. With the addition of bovine serum albumin (BSA), which may act as a secondary enhancer by stabilizing HRP, the detectability of the system has been further improved.

As alternative CL systems, acridinium esters are successfully used in automated clinical chemistry immunoanalyzers offering tremendous potentiality, however they are still unexplored for biosensing applications (Nakazono et al., 2017; Ma et al., 2017).

Recently, Shaap's adamantylene-dioxetane derivatives have been revisited to solve their main limitation, which is poor emission in water environment. For this purpose, new probes have been produced in which signal amplification was obtained by exploiting two approaches. In one case, the amantylidene−dioxetane was conjugated with a fluorescent acceptor that would significantly amplify the CL emission through an energy transfer mechanism, also providing shift of the emission wavelength to higher values. Alternatively, to achieve direct amplification, an electron-withdrawing group (EWG) was introduced in the molecule to increase the emissive nature of the benzoate species obtained during the chemiexcitation pathway of the probe. The efficiency of the probe was increased of more than 3 orders of magnitude with respect to standard, commercially available adamantylidene−dioxetane probes (Hananya et al., 2016).

Exploiting the adamantylidene−dioxetane molecular structure, thermochemiluminescent (TCL) compounds have been recently revisited as promising labels for biosensors. In these molecules, the

introduction of a fluorescent acridane moiety gave rise to self-luminescent molecules, in which light emission is simply triggered by heating (Di Fusco et al., 2015).

2.2 Fundamental update in analytical electrochemistry

A common definition of electrochemical sensing is the measurement of an electrically measurable signal generated by the redox reaction of an electroactive substance; in case of biosensors, the substance to detect is not electroactive *di per se*, but can produce or be associated to another electroactive specie by means of a biological element. The reaction generally happens on the surface of a so-called working electrode, which operates in conjunction with other two electrodes, the reference and auxiliary ones, forming an electrochemical cell where the redox reaction occurs as consequence of an electric potential applied to the electrodes. The signal magnitude of the resulting current is normally associated to the analyte concentration.

The principles of the electrochemistry using an electrochemical cell constituted of classical bulk electrode (e.g. platinum, gold) and Ag/AgCl/Cl^- reference electrode are well known, while the most modern miniaturised and nanomaterial-based sensors can show a different electrochemical behaviour. In the frame of miniaturised sensor, screen-printing technology has revolutionized the electrochemical sensors area because of its simplicity, cost-effectivity and versatility, being able to print, in a highly reproducible manner, many materials on a variety of substrates, and making possible the production of electrodes with different geometries, even custom-made. The technology consists of printing diverse conductive and non-conductive inks on alumina and plastic substrates, but the most attractive characteristic of these sensors is the possibility to easily modify the working electrode in order to enhance its electroanalytical performances (Kadara at al., 2009; Wang et al., 1998). Passing from solid metal electrodes to the printed ones, the electrochemical performance of these latter can be not the same. From the composition point of view, the SPEs are more similar to the carbon paste electrodes, being both constituted by a carbon powder with an organic binder (Fanjul-Bolado et al, 2008). Both components can affect the properties of the electrode: the binder, being non-conductive, can decrease the effective electron transfer rate constant due to the increase in polymeric domains and the reduction in conductive pathways (Choudry et al. 2010). On the other hand, the nature and amount of the carbonaceous particles and their size (nanodimensions such as for carbon nanotubes, graphene, carbon black, etc…), the roughness factor, the presence and accessibility of graphitic edge planes also strongly affect the electrochemical behaviour of SPEs, as demonstrated by numerous papers in literature (Wang et al., 1998; Kadara et al., 2009; Wang and Musameh 2004; Lin et al., 2004; Guan et al., 2005; Choudhry et al., 2010; Wang et al., 2014).

These characteristics, however, can be modified using several surface electrochemical or chemical pretreatment methods. These latter can increase the surface functionalities through the formation of new carbon–oxygen bonds that enhance the charge transfer, can provoke cracks that increase the roughness of the surface, can improve the wettability, reduce the extend of the organic layer and can promote a better exposure of graphite edges, improving the faradaic current. Lastly, also the printing process, especially the inks curing temperature, and the chosen electrochemical technique, can affect the performance of the SPEs (Setford et al., 1999; Morrin et al., 2003; Wang et al., 1996; Cui et al., 2001; Wei et al., 2007; Ghamouss et al., 2007).

Another critical part of the SPEs is the printed reference electrode (RE). The RE is an important component of any electrochemical cell; to be efficient, a reference electrode should have a stable potential. A traditional RE is isolated from the bulk solution by a glass frit or salt bridge (Ives and Janz, 1961). In the SPEs, the reference electrode is also printed using inks containing silver and/or silver chloride and is directly exposed to the measuring solution. Because of the absence of a liquid electrolyte containing Cl^-, the printed RE is considered as a pseudo-reference electrode and should be used in solutions with a fixed ionic strength, in order to avoid a shift of the working electrode potential. This phenomenon is more critical for potentiometric screen-printed sensors, however also in voltammetric techniques the stability of the reference electrode can affect the performance of the sensors. Thus, KCl should be added to the measuring solution in order to stabilise the potential of the RE (Inzelt et al., 2013).

In order to obtain the best analytical performances, all the above-mentioned characteristics should be studied and tuned for the particular analyte to be detected, but the advantages of easy handling, cost-effectiveness, need for very small sample volumes often without pretreatment, portability (even wearability), of these sensors (and related instrumentation) are worth to go forward with these studies.

3. RECENT TECHNOLOGICAL ADVANCEMENTS TO BOOST BIOSENSORS ANALYTICAL PERFORMANCES AND PORTABILITY

During the last decades, biosensors have dramatically progressed through the introduction of novel (nano)materials and technologies, which provided new assay formats, improved figures of merit and miniaturized portable devices.

Nanoscale materials such as nanoparticles (NPs), nanocluster, nanocomposites, quantum dots (QDs), carbon dots, graphene and graphene oxide (GO), as well as several nanocomposites, supply key elements for fine-tuning (bio)sensors, acting as signal amplification structures, catalysts, reductants,

luminophores, energy acceptors, or bioreceptor immobilization platforms, and also fostering the sensitivity, selectivity and stability of the developed nanosensors.

The trends of the last 10 years highlight graphene as the rising star in the plethora of nanomaterials employed in (bio)sensing (Cinti and Arduini, 2017). Indeed, carbon nanomaterials offer several attractive features, such as easy and efficient surface grafting and other special physical properties deriving from the unique π-π surface conjugation ability, as well as by the high number of defect sites. Graphene and its derivatives, including GO and reduced GO (rGO), are considered among the most promising materials in the twenty-first century, thanks to their astonishing features such as large surface area, thermal conductivity, room-temperature electron mobility, mechanical strength, and ease tailorability. Beyond carbon-based nanomaterials, metal NPs, such as Au NPs, Ag NPs, bimetallic NPs, and metal oxide NPs have demonstrated the capability to furnish peculiar features to biosensors, allowing for a smart detection. For instance, in case of CL detection, metallic NPs have shown to possess peroxidase-like activities enhancing the CL emission from the luminol/H_2O_2 system (Li et al., 2014). Moreover, they encompass their treasured electrochemical and optical properties as well as the suitability to act as labels in immunoassays, to immobilise the biocomponent, and to increase the storage stability by creating a favourable environment in both photon and electron-based biosensors.

Parallel developments in microelectronic, microfluidic and printing technologies have allowed for the creation of disposable, miniaturized devices that combine various assay steps into a compact space for delivering both electrochemical and CL miniaturised biosensors with attractive features for market entry (Mazzaracchio et al., 2019; Nascetti et al., 2019). Herein, we highlight the most promising technological advancements in chemiluminescent and electrochemical biosensors capable to improve the analytical features of the devices in terms of low detection limit, wide linear range, and improved robustness.

In the following paragraphs, the main recent trends are highlighted, reporting several examples of CL and electrochemical biosensors, which main features are also summarized in Table 1.

3.1 Technological advancements in chemiluminescent biosensors

The main challenge in CL is to improve the luminescence quantum yield still relatively low by developing new CL reagents cocktails and catalyst emitting in different part of the visible spectrum.

Nanomaterials are being extensively employed to improve CL-based bioassays, acting as catalyst, emitter, or energy acceptor (Li et al., 2014; Tiwari and Dhoble, 2018). Starting with the pioneering work showing the ability of metal NPs to catalyze CL reactions (Zhang et al., 2005), nanoluminophores with excellent emission properties were developed by grafting CL reagents on the surface of AuNPs

(Zhang et al., 2013), with further improved CL efficiency obtained upon additional functionalization with metal complexes (Huang et al., 2018b). With this approach, immunoassays for human IgG and other proteins have been developed, reaching LODs down to subfemtomolar levels. In addition to metal NPs, other nanomaterials, such as QDs and carbon-based nanomaterials, have been exploited as catalysts or emitters for improved CL biosensing strategies, although their mechanism of action is still under investigations in many cases (Wang et al., 2019).

Composite nanomaterials have recently attracted much attention, owing to their superior CL properties over their monomaterial counterparts. For example, Cu/Co bimetallic manomaterials, which provided enhanced catalytical ability thanks to the two metals synergistic effect, were employed as the nanocatalysts for the CL reaction, enabling detection of cancer cells down to 270 cells mL^{-1} in an aptamer-based assay (Li et al., 2018). Graphene oxide-based composite materials (e.g., metal-GO or bimetallic-GO) have also been prepared to improve the GO catalytic activity towards CL reactions. With this approach, a dramatic enhancement of the luminol−H_2O_2 and lucigenin−H_2O_2 CL reactions was obtained by coupling Co^{2+} and GO. Theoretical studies revealed that the coupling between metal ions and GO induced effective polarization charges, facilitating the generation of several radicals that drive the CL reaction. However, applicability in biosensors has not been demonstrated yet (Wang et al., 2017).

Nanotechnology can bring a significant progress in CRET, which has been poorly exploited due to the small energy transfer efficiency and to the limited number of effective CL donors and energy acceptors. For example, a turn-off CRET-based sandwich immunoassay was developed for copeptin, a surrogate marker for acute myocardial infarction, exploiting TiO_2 NPs functionalized with a porphyrin derivative and N-(4-aminobutyl)-N-ethylisoluminol (TiO_2-TCPP-ABEI nanoluminophores) as CL emitter, while AuNPs were employed as energy acceptor. The assay provided a wide dynamic range (5×10^{-12} - 1×10^{-9} g mL^{-1}) with a LOD of 1.54×10^{-12} g mL^{-1}, which was superior to previously reported CL-based immunoassays. (Shu et al., 2019).

Other novel materials, such as metal-organic frameworks (MOFs) and layered double hydroxides (LDHs) have very recently appeared on the scene of CL biosensing, opening a new perspective for further improved analytical performance. As an example, Zhu et al., developed a CL-based biosensor for one-step and rapid detection of glucose in human urine down to 50 nM, exploiting a 2D-MOF nanosheet with peroxidase activity functionalized with luminol and glucose oxidase (GOD), to yield a Co-TCPP(Fe)@luminol@GOD composite material able to generate a CL signal by simple addition of the sample (Zhu et al., 2019a).

In parallel with advances in nanomaterial science that boosted CL-based biosensors sensitivity, great advancements towards their point-of-need applicability have been achieved thanks to technological

innovation, providing miniaturized ultrasensitive photon detectors and novel portable analytical formats (Roda et al., 2011; Mirasoli et al., 2014a). Indeed, CL is particularly suited for miniaturization, as it does not require wavelength selection of the acquired signal, nor specific geometries for the measurement cell (Roda et al., 2016). The only main requirement is maximizing photon collection efficiency, which is easily obtained in "contact" geometries, in which the measurement cell is in direct contact with the photodetector (Roda et al., 2011). The fast innovation in electronics has enhanced the development of miniaturised transducers for point-of-need CL biosensors, such as cooled slow-scan or intensified CCD sensors (Zangheri et al., 2019), a smartphone CMOS sensor (Rezazadeh et al., 2019; Roda et al., 2019) and thin film photosensor arrays (Soares et al., 2017; Mirasoli et al., 2014b). Also in this field, nanotechnology could open the door for novel opportunities. Recently, a miniaturized photosensor was obtained by in situ synthesis of cadmium sulphide nanowires on the gold surface of an interdigitated electrode. The photosensor provided a LOD of 3.2 ng mL^{-1} in a CL immunoassay for carcinoembryonic antigen, which is similar to that obtained with a commercial photomultipler tube-based luminometer (Im et al., 2017).

Apart from the photodetector miniaturization, the biosensor analytical format plays a crucial role for its point-of-need applicability. The main critical point of CL biosensors is the requirement for a complex set of ancillary equipment for handling reagents and washing steps in the microfluidic network. The cheapest and most affordable approach is based on cellulose-based supports, such as micro paper-based analytical devices (μPAD) and lateral-flow immunoassay (LFIA), which has deservedly become a current trend in the field of real-time analysis (Zhu et al., 2019b). Several CL paper-based biosensors have been developed, exploiting various solutions to provide multiplex analysis. For example, a double-layered three-dimensional (3D) microfluidic network was exploited for temporizing reagents delivery, thus developing a multiplex CL enzyme assay for detecting glucose, lactate, choline, and cholesterol with LODs of 8 μmol L^{-1}, 15 μmol L^{-1}, 6 μmol L^{-1}, and 0.07 μmol L^{-1}, respectively (Li et al., 2019). Furthermore, to overcome the shortcomings of natural enzymes as labels, Pt NPs with catalytic activity were employed as enzyme-mimic label in a CL LFIA, providing a far higher thermal stability than HRP at room temperature, and displaying a LOD of 1 mIU mL^{-1} for human chorionic gonadotropin (hCG) (Park et al., 2015). As an alternative, thermochemiluminescent (TCL) silica- and polymer-based NPs are promising labels for miniaturized biosensor formats, as they combine high detectability of CL with reagentless trigger of the light emission, which is simply elicited by heat (Andronico et al., 2018; Roda et al., 2019).

3.2 Technological advancements in electrochemical biosensors

The advanced technologies such as nanomaterial, printing and microfluidic technologies boosted the electroanalysis towards a true Renaissance, conferring new features to the electrochemical (bio)sensors (Escarpa et al., 2012) including low detection limit, high sensitivity, miniaturisation, and low sample volume.

In the field of electrochemical biosensor, the use of graphene has allowed to design smart electrochemical biosensors thanks to the polyedric features of this nanomaterial, such as the tailorability of the electrochemical properties of the developed biosensor. Indeed, the metallic impurities present in graphene as well its structure, i.e. single or multi layers, are able to affects the electroanalytical response (Ambrosi et al., 2012a, 2012b; Kampouris et al., 2010, Goh and Pumera, 2010). In addition, the amount of oxygen and the number of defect sites have a high effect on the electrochemical behaviour, improving e.g. electron transfer and allowing for low detection limit of the target analyte (Ambrosi et al., 2014).

Furthermore, the 2D structure of graphene has been exploited to use graphene as label or as loading agent for biomolecules and inorganic nanomaterials thanks to its high surface area and easy functionalization.

One of the first enzymatic graphene-based biosensors has been reported by Ping et al., which developed a glucose biosensor by the electrodeposition of reduced graphene-oxide and immobilisation of glucose oxidase via cross-linking method (Ping et al., 2011). The presence of graphene demonstrated the detection of enzymatic by-product hydrogen peroxide at low negative applied potential (-0.2 V vs Ag/AgCl), allowing for glucose quantification with a wide linear range up to 12 mM and detection limit equal to 1.0 µM.

In the immunosensor field, graphene was exploited for its double function: i) improvement of the electrochemical performances and ii) loading of antibodies/enzymes for the enhancement of a signal output. For instance, graphene oxide was used as substrate to immobilize the enzyme horseradish peroxidase and the antibody $p53^{392}Ab_2$ for the detection of the tumor suppressor and transcriptor factor p53(392) with a range up 2 nM and low detection limit equal to 0.01 nM, which is 10-fold lower in respect to the detection limits of established sensors using peroxidase-streptavidin-biotin-$p53^{392}Ab_2$ (Du et al., 2011).

The characteristic of graphene oxide nanoplatelets, namely inherently electroactive, was exploited to design an interesting DNA sensor for the detection of single-nucleotide polymorphism by following the interactions between graphene oxide nanoplatelets and DNA strands. The strategy of the detection relays on the different binding ability of single-stranded and double-stranded DNA towards graphene oxide nanoplatelets and the stronger ability of graphene to conjugate ssDNA with respect to dsDNA. As results, the non-complementary target yielded a higher voltammetric signal than the

complementary target (Bonanni et al., 2012), with a detectable difference between the wild-type and mutant at 10 nM. Beyond graphene, gold nanoparticles are the most employed nanoparticles also in the realization of electrochemical biosensors, followed by Silver- and Platinum-NPs. As an example, gold nanoparticle-based sol-gel stabilised with polyvinylpyrrolidone was utilised as matrix for tyrosinase enzyme immobilisation for the detection of catechol under µM level with improved storage stability up to 6 weeks (Singh et al., 2013).

Metallic nanoparticles were also used as label to evaluate the reaction between the biocomponent and the target analyte. For instance, the specific interaction between thymine and Hg^{2+} was exploited for the Hg^{2+} detection, forming the complex thymine-Hg^{2+}-thymine together with gold nanoparticles synthesized in loco as signal reporter, and using stripping voltammetry as detection technique (Tang et al., 2014). Silver nanoparticles have been adopted in an aptamer assay for *S. aureus*, by using a biotinylated primary anti-S. aureus aptamer onto streptavidin-coated magnetic beads as the capture agent, and a second anti-S. aureus aptamer conjugated to AgNPs as the detection agent. The binding between the aptamer and bacteria was quantified by anodic stripping voltammetry of Ag ions, reaching a detection limit of 1 CFU mL^{-1} (Abbaspour et al., 2015). Platinum nanoparticles encapsulated in metal–organic frameworks have used for telomerase activity evaluation following their electrocatalysis, observing a linear range from 500 to 10^7 cells mL^{-1}, with the activity calculated in a single cell equal to 2×10^{11} IU (Ling et al., 2016).

Gold nanoparticles have been also exploited as anchor points for the attachment of the thiol-extremity of DNA probes, as well as to improve the electrochemical performances as in the case of ss- and ds-DNA sequence detection of HIV in serum samples. The configuration of a miniaturised sensor combined with DNA probe and gold nanoparticles allowed detection limits of 3 and 7 nM, for ss and ds sequences, respectively (Cinti et al., 2018). One of the main features of electrochemical biosensor relies on the delivery of highly cost-effective devices thanks to the use of printing technology for their production. In the continuously growing of 2D printing technology field, screen-printing, ink-jet, roll-to-roll, sheet-to-sheet are the main types selected for device production. If the ink-jet printing is the most used in printed electronics, screen-printing remains the preferred one in manufacturing process of electrochemical sensor, being able to fabricate a huge number of sensors in few hours. Screen-printed electrodes have been widely used in the environmental, biomedical, and agrifood sectors for the detection of several analytes including pesticides, chemical and biological warfare agents, toxins, glucose, lactate, in a plethora of samples. For instance, gold screen-printed electrode has been modified with DNA-based aptamer for a single-step detection of *B. anthracis* spore simulant (*B. cereus* spore) using an impedimetric label-free approach. Under the optimized conditions, *B. cereus* spores were detected with a linear range between 10^4 CFU/ml and 5×10^6 CFU/ml and a detection limit of

3×10^3 CFU/mL, providing an aptasensor combined with a portable instrument for an on-site label-free measurement of *B. anthracis* spore simulant (Mazzaracchio et al., 2019). In the case of gold printed electrodes, the self-assembled monolayer technique is used to immobilise the biocomponent thanks to the thiol-gold bonding; in the case of graphite-based screen-printed electrode, cross-linking based-immobilisation is often chosen. As an example, a graphite screen-printed electrode was modified by drop casting with a nanocomposite constituted of cobalt phthalocyanine and carbon black followed by the immobilisation of butyrylcholinesterase enzyme using glutaraldehyde, Nafion, albumin bovine serum, allowing for organophosphorus pesticide detection at ppb level (Cinti et al., 2016a).

The possibility of using miniaturised sensor with low volume sample has also furthered the development of lab on a chip combining microfluidic with electrochemical miniaturised biosensors. Screen-printed electrodes modified with acetylcholinesterase (Yoon et al., 2014) or butyrylcholinesterase (Arduini et al., 2012a) were integrated in microfluidic chip to identify the presence of nerve agents in liquid solution or in vapour phase. However, the designed microfluidic devices required the addition of solution containing the reagents, external pump or the intervention of the operator.

In the era of sustainability, the electrochemical printed biosensors have rediscovered an old material, i.e. paper, which has opened a new research line delivering electrochemical paper-based analytical devices (ePADs). These sustainable analytical tools are able to treat the sample, store the reagent, make the measurement, being the electrochemical cell printed directly on paper, without any external pump. ePADs have initially attracted a huge attention in biomedical field, being able to match the ASSURED criteria has been reported by Henry group, which designed microfluidic channels on filter paper by using photolithography, and electrochemical cells on filter paper by using the screen-printing technology. For selective quantification of glucose, lactate and uric acid, glucose oxidase, lactate oxidase, and uricase enzymes were entrapped in three different zones of filter paper to detect these analytes, by easily adding the biological liquid sample in the centre zone of the device (Dungchai et al., 2009). In this case, an external pump is not required because the solution flow is driven by the capillarity properties of the paper, and the reagents are not added by the operator, but previously entrapped in the cellulosic network of the paper. For ePADs, both lateral and vertical flow microfluidic have been exploited, thanks to the capability of the electrochemical sensors to work in different configurations. Furthermore, the wax-printing to create the paper-based microfluidic, combined with the screen-printing technique to print the electrochemical cell, are capable to deliver a paper-based analytical tool characterised by low cost and easiness to use, where only the addition of the few μL of the sample is the task required to the operator.

As an example of lateral flow, an integrated paper-based screen-printed electrochemical biosensor device able to quantify nerve agents was reported. In detail, a paper-device with dual electrochemical measurements of butyrylcholinesterase activity was designed to evaluate the response in presence and in absence of polluted water samples. By just adding few μL of the sample on a dedicate zone that wets both the strips, it is possible to detect a nerve agent simulant down to 3 μg/L, delivering a fast and easy to use analytical tool (Cinti et al., 2017).

The foldability of the paper combined with the flexibility of the electrochemical measurement has allowed the design of an attractive origami paper-based device. To this regard, a three-dimensional origami paper-based device for the detection of several classes of pesticides by combining different enzyme-inhibition biosensors was developed. By combining different office paper-based screen-printed electrodes with multiple filter paper-based pads, and folding, cutting and unfolding them, it is possible to measure different classes of pesticides at ppb level just directly adding the sample without any previous sample treatment and exploiting the vertical microfluidic of the eco-designed device (Arduini et al., 2019).

Furthermore, the combination of different technologies such as screen, wax and 3D-printing, allowed the delivery of smart point of care devices for biomedical application. For instance, Scordo et al. reported the first example of a rapid and easy to use paper-based printed sensor embedded in a 3D printing device for the measurement of butyrylcholinesterase activity in serum samples. This analytical tool encompasses paper-based microfluidic using wax printing, screen-printing to print the electrodes, and stereolithography using 3D printing technology for a customised fabrication of the holder. Butyrylcholinesterase activity was measured in serum with a linear range up to 12 IU/mL and a detection limit of 0.5 IU/mL, demonstrating its suitability as a point of care, being normal value range of comprised between 5.9 and 13.2 IU/mL (Scordo et al., 2018).

4. ELECTRON-BASED VS PHOTON-BASED BIOSENSORS: an experimental challenge

In the previous scenario we have highlighted the major trends in CL and electrochemical biosensor field, demonstrating how the cutting-edge technologies impact the dimension, the cost, the sample volume and treatment, and the analytical performances of these devices. However, the reported literature demonstrated the relevant features of both CL and electrochemical biosensors, without revealing the best transducer for highly sensitive, cost-effective and on-site measures. To face this challenge, a direct comparison in the same working condition is needed.

Herein, we report the experimental results related to H_2O_2, HRP, IgG, and glucose measurements by using some of the above technologies, and sharing the same reagents to give a correct competition between photons and electrons. Protocol schemes are depicted in Figure 3.

4.1 Materials and Methods

4.1.1 Reagents

Peroxidase from horseradish Type VI-A (1080 U mg^{-1}) was purchased from Sigma-Aldrich. For HRP electrochemical measurement, a supersensitive solution ready to use containing TMB + hydrogen peroxide in buffer was used (Sigma Aldrich). For HRP CL measurement, black (with clear bottom for contact imaging) 96-multiwell plate (Thermo Fisher Scientific) and the CL substrate Super Signal ELISA Femto (Thermo Fisher Scientific) were employed. Magnetic beads (MBs) coated with Goat Anti-Rabbit IgG were supplied as a suspension containing 3.65×10^{10} beads mL^{-1} by New England Biolabs (Ipswich, MA, UK). Hydrogen peroxide standard solution was purchased from WWR Prolabo Chemicals.

4.1.2 Instrumentation and sensors for CL measurements

For CL measurements in a benchtop configuration, a PMT based microtiter reader (Varioskan Flash multimode reader, Thermo Fisher Scientific, Waltham, MA, USA) was employed, which displays a sensitivity of <7 amol ATP/well and a dynamic range >7 decades, as measured by flash ATP reaction in a 384-well plate. As a portable device, a thermoelectrically cooled portable ATIK 11000 CCD camera (ATIK Cameras, New Road, Norwich) connected to a light-tight dark box was employed. The CCD camera, which is equipped with a large format, high resolution monochrome CCD sensor (Kodak KAI 11002, sensor size 37.25 ×25.70 mm) cooled by a two-stage Peltier element to reduce thermal noise, was either coupled with an objective (Computar 2/3 in. 8 mm, f1.4, obtained from CBC AMERICA Corp., Commack, NY), or employed in contact imaging approach, employing a polymethylmethacrylate fiber optic faceplate (size 26 × 26 × 13 mm, Edmund Optics, Barrington, NJ), as previously reported (Zangheri 2019).

In all measurements, data were subtracted of the blank signal.

The contact lensless imaging CCD-based device has been designed to maximize the photon collection efficiency, as previously reported (Roda et al., 2011). A theoretical evaluation of the detectability of a model analyte, such as luminol, can be performed. Considering that in a back-illuminated cooled CCD camera each pixel is characterized by an electronic readout noise of about 10 electrons, that thermal noise is negligible when the sensor is cooled down to -20°C, and that the quantum efficiency (i.e., the ratio of generated electrons over impinging photons) is at least 50%, about 60 photons are necessary

for obtaining a signal-to-noise ratio of 3. Assuming a 180° light collection angle typical for a contact imaging configuration, the number of photons doubles to 120. As the the luminol/H_2O_2 CL system displays a Φ_{CL} of about 1% in aqueous solutions, about 1,2 x10^4 luminol molecules should undergo oxidation to produce this photons output. Therefore, if we consider a 1-mm^2 sensing area (corresponding to 12000 pixel for a pixel size of 9x9 µm), 200 amol of CL products can be detected in 1s.

4.1.3 Instrumentation and sensors for electrochemical measurements

For electrochemical measurements, a laboratory potentiostat Autolab electrochemical system equipped with PGSTAT-12 and GPES software (Eco Chemie, Utrecht, The Netherlands) or a portable potentiostat equipped with PS Trace 3.0 software (Palm Sens, The Netherlands) were employed.

Polyester-based screen-printed electrodes (SPEs) were produced with a 245 DEK (Weymouth, UK) screen-printing machine. Graphite-based ink (Electrodag 423 SS) from Acheson (Milan, Italy) was used to print both the working and auxiliary electrode. Silver/silver chloride ink (Electrodag 477 SS) was used to print the pseudo-reference electrode. The substrate has been a flexible polyester film (Autostat HT5) purchased from Autotype Italia (Milan, Italy). The diameter of the working electrode was 0.3 cm resulting in a geometric area of 0.07 cm^2. SPEs were then modified by drop casting with 6 µl of Carbon Black (CB) dispersion 1 mg/mL (Arduini et al., 2012 b) (for HRP and IgG measurement) or with dispersion 1 mg/ml of Carbon Black + Prussian Blue nanoparticles (CB/PBNPs) for H_2O_2 measurement (Cinti et al., 2014).

For the CB/PBNPs powder production, we followed our previous procedure (Moscone et al., 2001), where graphite was substituted by CB. CB/PBNPs powder was finally used to produce dispersion at a concentration of 1 mg in 1 mL of a dimethylformamide:water (1:1) mixture used as solvent, and then sonicated for 60 min at 59 kHz. The dispersion was used for modifying bare SPEs via drop-casting. In detail, a small volume (6 µL) of the CB/PBNPs dispersion was cast onto the working electrode surface in three steps of 2 µL each (CB/PBNPs-SPE).

4.1.4 Horseradish peroxidase measurement

Peroxidase was serially diluted in the range 2 x 10^{-15} to 6 x 10^{-12} mol L^{-1} in 0.1 M phosphate buffered saline (PBS) pH 8 and analysed by CL or electrochemical detection.

For CL detection, 20 µL of HRP solution was dispensed in the wells of the multiwell plate, then 80 µL of Super Signal ELISA Femto was added. Photon emission was measured with the Varioskan Flash reader or the CCD camera with a signal integration time of 1 s or 120 s, respectively.

For HRP electrochemical measurement, 125 µL of supersensitive solution (TMB + hydrogen peroxide in buffer) and 10 µL of HRP enzyme at different concentration were added on the surface of the SPE. After 10 min 25 µL of NaN_3 0.024 M was added to stop the reaction and the current was measured in chronoamperometry using SPE modified with CB and the following conditions: applied potential= -100 mV, duration time= 60 s, interval time= 0.1 s. The current was measured at 60 s.

4.1.5 Hydrogen peroxide detection.

Calibration curves for H_2O_2 were prepared in the range 1x 10^{-8} – 1,25 x10^{-3} M in 0.1 M phosphate buffered saline (PBS) pH 8.

Hydrogen peroxide was detected by CL employing HRP as a catalyst. In particular, 20 µL of HRP solution (1 x 10^{-6} g mL^{-1} in PBS) and 40 µL of the Super Signal ELISA Femto kit (only the Luminol component) was dispensed in the wells of a 96-well plate. Upon addition of 40 µL of the H_2O_2 solution, photon emission was measured in the Varioskan Flash reader or the CCD camera with a signal integration time of 1 s or 120 s, respectively.

Hydrogen peroxide was electrochemically detected by direct reduction. Briefly, 70 µL of hydrogen peroxide standard solution was added on the surface of a SPE modified with CB/PBNPs. The current was chronoamperometrically measured using the following conditions: applied potential= -100 mV, duration time= 60 s, interval time= 0.1 s. The current was measured at 60 s.

4.1.6 Paper-based enzyme biosensor for glucose detection

A Paper-based Analytical Device (PAD) was designed employing Labor (67 g/m^2) filter paper, purchased from Cordenons (Italy), as a substrate. ColorQube 8580 office printer from Xerox (USA) was used to print a specific hydrophobic pattern on paper, previously designed using a drawing software (Adobe Illustrator). The wax-printed paper was then placed in an oven for 2 min at 100 °C, allowing the printed wax to penetrate the substrate producing a hydrophobic boundary around hydrophilic areas. Glucose Oxidase enzyme (GOx) was immobilised onto wax-modified filter paper, in which a hydrophobic pattern was exploited to entrap the GOx solution into the desired area. 4 µL of GOx solution (50 U mL^{-1} in 0.05 M phosphate buffer pH = 6 containing 0.1 M KCl) were drop-cast onto the PAD hydrophilic area and solvent was let evaporate.

Only for electrochemical measurements, GOx-containing PADs were fixed by means of a common glue onto CB/PBNPs-modified office paper sensors, produced as follows: conductive inks were used to print a three-electrode system onto the wax-modified office paper sheets, as previously described (Cinti et

al., 2016b; Cinti et al., 2019), then the working electrode surface was modified with 6 µL of a CB/PBNPs (1 mg/mL m/v), by drop-casting 2 µL for three times.

For assay execution, 40 µL of glucose solution (concentration range 5 x 10^{-6} – 2,50 x 10^{-4} M in phosphate buffer) was added and the CL or electrochemical detection was achieved.

For CL detection 40 µL of Super Signal ELISA Femto was added and photon emission was measured employing the CCD camera with a 120-s signal integration time.

Electrochemical detection was carried out by recording the amperometric signal. Applied potential= 0 mV, duration time= 300 s, interval time= 0.1 s. The current was measured at 300 s.

4.1.7 Immunoassay for IgG detection

A model non-competitive sandwich type immunoassay for IgG quantitative detection was set up. Goat Anti-Rabbit IgG magnetic beads were used as a solid phase. For the assay, 10 µL of magnetic beads suspension and 200 µL of solution containing Rabbit IgG at different concentrations were added in different tubes and incubated for 30 min. Upon washing, 200 µL of Goat Antirabbit-HRP diluted 1:400 v/v were added to each tube and incubated for 30 min. After the washing step, magnetic beads were re-suspended in 50 µL of phosphate buffer, and either CL or electrochemical detection was performed.

For CL detection, 20 µL of MBs suspension was dispensed in the wells a multiwell plate and, upon addition of 60 µL of Super Signal ELISA Femto, photon emission was measured in the Varioskan Flash reader or the CCD camera with a signal integration time of 1 s or 120 s, respectively.

For electrochemical detection, 20 µL of MBs suspension were transferred onto the surface of a CB-modified SPE using the magnetic support for concentrate the beads onto the working electrode. The sandwich-complex was revealed by adding 70 µL of the substrate supersensitive solution TMB + hydrogen peroxide ready-to-use. The product was chronoamperometrically measured using the following conditions: applied potential= -100 mV, duration time= 60 s, interval time= 0.1 s. The current was measured at 60 s.

5 RESULTS AND DISCUSSION

A series of experiments were carried out to directly compare the performance of CL and electrochemical detection in different bioassay formats, employing the same reagents and when possible, the same experimental conditions. The optimal conditions for each detection principle were in fact established, in each experiment, based on the expertise of the two research groups, taking advantage of the availability of optimized protocols and of state-of-the-art instrumentation available in their laboratories, in order to challenge each detection principle while operating at its best

possibility. With this approach, it was possible to highlight for both methods their strengths and weaknesses in biosensing**.**

In HRP assay, two types of instrumentation were employed: a state-of-the-art laboratory benchtop instrumentation and a portable instrumentation suitable for Point-of-need applications, with the aim of evaluating the performances of the portable and laboratory benchtop instrumentation with the same transduction principle. In all the experiments, the limit of detection (LOD) was calculated as the analyte concentration corresponding to the mean blank signal plus three times its standard deviation; the limit of quantification (LOQ) was similarly calculated employing ten times the blank standard deviation, while the linear range was evaluated by applying the analysis of variance (ANOVA). Table 2 reports the summary of calculated values.

5.1 HRP measurement

HRP is one of the most frequently employed enzyme label in biosensors, its detectability being strictly related to the achievement of a low LOD, keeping a reasonable linear range. The calibration curves were constructed for HRP enzyme, to evaluate detectability and linear dynamic range for the enzyme detection.

The HRP concentration detection involves of course the measurement of its activity under a fixed incubation time, working in a substrate excess; however, the best choice should be an enzyme with high purity and high specific activity, thus producing an adequate signal in a short time using a small amount of label.

For CL-based detection (Figure 4A), the calibration curve obtained at the Varioskan showed a LOD of 2 x 10^{-15} mol L^{-1} (corresponding to 4.5 x 10^{-20} mol/well), a LOQ of 9 x 10^{-15} mol L^{-1}, with a linear range extending up to 1 x 10^{-9} mol L^{-1}. Employing portable instrumentation, a very slight increase of the LOD value was observed (7 x 10^{-15} mol L^{-1} for contact imaging, 1 x 10^{-14} mol L^{-1} for optics-based imaging, corresponding to 13 x 10^{-20} mol/well and 23 x 10^{-20} mol/well, respectively), thus confirming high HRP detectability also in POCT configuration. Interestingly, the CCD-based imaging approach provided the highest signal-to-noise values at each HRP concentration, thus providing higher assay sensitivity, owing to the higher calibration curve slope.

One peculiar feature for CL detection is the possibility to extend the dynamic range of the assay by changing the signal integration time, particularly when imaging is performed. Indeed, by using high integration times for low HRP concentrations and gradually decreasing the integration times at higher HRP concentration, pixel saturation effects can be avoided, thus maintaining low LOD values, while further extending the dynamic range of the assay.

The electrochemical calibration curve obtained, reported in Figure 4B, showed a LOD of 2 x 10^{-15} mol L^{-1} (corresponding to 20 zeptomoles) and a LOQ of 3,5 x 10^{-15} mol L^{-1}, with a first linear range extending from 0.34 up to 3.5 x 10^{-14} mol L^{-1} and a second linear range extending from 0.45 up to 19 x 10^{-12} mol L^{-1}. Employing the portable instrumentation, a slight increase of the LOD (3 x 10^{-15} mol L^{-1}) and LOQ (9 x 10^{-15} mol L^{-1}) values was observed (corresponding to 3.0 x 10^{-20} and 9.0 x 10^{-20} mol/well, respectively). The laboratory instrument provided the higher sensitivity at the lower concentration range. This behaviour is ascribed to the presence of additional electronic components in laboratory benchtop instrumentation able to filter the noise at nA signal output, giving higher signal/noise ratio.

To evaluate the ability of CL or electrochemical measurements to distinguish between slightly different analyte concentrations, i.e. their sensitivity, the slope of the calibration curve was divided by the average standard deviation measured in the points of the curve. For CL detection performed with the Varioskan instrumentation a value of 3000 mol^{-1} was obtained, while electrochemical measurements performed with the Autolab provided a value of 21000 mol^{-1} in the first part of the curve and 30 mol^{-1} in the second linear range. Therefore, electrochemical measurements provided higher discrimination ability at lower analyte concentration, while CL was superior in the higher concentration range.

5.2 Hydrogen peroxide detection

Hydrogen peroxide is involved in many coupled enzymatic reactions, being the enzymatic by-product of the oxidase enzymes; therefore many analytes have been detected via its measurement with different approaches.

The results obtained using CL sensor (Figure 4C), show a LOD of 1 x 10^{-7} mol L^{-1} and a LOQ of 4 x 10^{-7} mol L^{-1} (corresponding to 4 x 10^{-12} mol/well and 16 x 10^{-12} mol/well, respectively), with a linearity extending up to 1,25 x 10^{-3} mol L^{-1}. Results obtained using laboratory benchtop instrumentation and SPE modified with CB/PBNPs (Figure 4D) demonstrated a lower detectability (i.e., LOD equal to 3 x 10^{-6} mol L^{-1} and LOQ equal to 7 x 10^{-6} mol L^{-1}, corresponding to 210 x 10^{-12} mol/well and 500 x 10^{-12} mol/well, respectively) with a narrower linear range up to 5 x 10^{-4} mol L^{-1}. However, the higher detectability observed with the CL device required the use of a biocomponent, i.e. HRP enzyme, while the electrochemical detection can be considered more sustainable and robust, since only phosphate solution is necessary for the measurement. Furthermore, the absence of biocomponent delivers a sensor characterized by high storage stability. This latter is a key feature for the market, because a low storage stability is very often the reason of the gap between the research field and the market: a sensor that requires low temperature for maintaining its performances and it is stable just for few days is not suitable for market entry.

.

5.3 Paper-based glucose oxidase biosensor

As reported in the introduction, glucose biosensor is without any doubts the most investigated biosensor type for its high analytical performances in terms of detectability, high working and storage stability, as well as for his utility in diabetes management.

Herein, we compare sustainable paper-based devices using CL or electrochemical transduction with portable instrumentation, with the main idea that paper-based devices should be able to fit the ASSURED criteria established by WHO.

Using CL configuration, the calibration curve reported in Figure 5A showed a LOD 1.7 x 10^{-5} mol L^{-1} and linearity up to 2 x 10^{-3} mol L^{-1}.

In case of electrochemical detection, a wider linear range up to 1 x 10^{-2} mol L^{-1} was observed, described by the equation y = (0.55 ± 0.02)x + (0.2 ± 0.1), with a r^2 = 0.966 and a LOD equal to 4 x 10^{-5} mol L^{-1} (Figure 5B).

5.4 IgG quantification

Being IgG the primary response of the immune system, the IgG detection furnishes a well-established analytical tool to measure infection. To enlarge the competition between photons and electrons, a typical sandwich immunosensor was designed for IgG measurement using magnetic beads as solid support for the immunological sandwich.

A typical calibration curve obtained for CL detection (Figure 5C) displays a linear portion at lower analyte concentrations, with a saturation effect at higher concentrations. From this curve, a LOD of 1.2 x 10^{-14} mol L^{-1} and a LOQ of 1.6 x 10^{-13} mol L^{-1} were calculated. In case of electrochemical detection, a LOD of 1.2 x 10^{-13} mol L^{-1} and a LOQ of 2.7 x 10^{-13} mol L^{-1} were calculated, demonstrating similar results using the same measurement time.

6. CONCLUSIONS

The experimental measurements performed in this paper have been carried out employing the same reagents, and, in almost all circumstances, the same conditions. In some cases, however, the optimal conditions were chosen in order to allow both methods to operate at their best possibility, according to the background of the research groups, of the availability of optimized protocols and of the instrumentation existing in their laboratories.

The obtained results demonstrated that biosensors based on amperometric and CL detection principles, despite offering similar detectability and comparable analytical performance, display subtle

differences in some practical experimental aspects, permitting to indicate them in complementary application fields. Generally, CL is characterized by slightly lower LOD values and wider dynamic ranges, even though this is not always confirmed, and, in all experiments, quite small differences have been observed. In particular, while comparable detectability was observed when comparing the two transduction principles in HRP detection and in enzyme- and immuno-based biosensors, significantly lower LOD and LOQ values were obtained with CL-based detection of hydrogen peroxide with respect to amperometric detection. This could be ascribed to the fact that enzyme catalysis was employed in CL-based assay, while H_2O_2 was directly detected at the electrode

One peculiar characteristic of CL is the higher assay sensitivity i.e. slope of the dose-response curve observed with portable devices with respect to benchtop instrumentation, as well as the possibility to extend the assay dynamic range by varying the signal acquisition time.

Nevertheless, as high detectability in CL imaging is obtained at increasing acquisition times, in the order of minutes, with slow-scan cooled CCD cameras, this is a disadvantage with respect to amperometric measurements that can reach comparable LODs with shorter acquisition times. Nevertheless, this limitation will probably be soon overcome with technological advancements for enhanced CCDs, complementary metal oxide semiconductor (CMOS) and thin-film photosensors.

The shorter analysis time will allocate electrochemical biosensors in the real-time monitoring such as wearable biosensors. On the other hand, CL based biosensors should be more devoted to POCT for clinical biomarkers where the detectability is more important (Roda et al., 2018).

Although not explored in our experiments, multiplexing ability is also an important feature for biosensors market penetration, especially in the view of their application in personalized medicine and companion diagnostics. With this respect, both electrochemical and CL biosensors, that can be arranged in arrays (or, for CL, also exploit imaging), are suitable (Zangheri et al., 2015; Li et al., 2019).

The challenge reported here from analytical point of view demonstrated that these biosensors have competitive and similar analytical features, and between photons and electrons the challenge is still open, especially when comparison is performed on the same target analyte and biosensing principle.

On the contrary, significant differences can be evidenced in other applications, in which each transduction technology offers unparalleled features.

Indeed, optical methods, and particularly BL/CL detection, offer unique possibilities for *in vivo* and *ex-vivo* imaging, a powerful tool for monitoring of several physiological and pathological processes, such as inflammation, tumour growth, and drug delivery. Furthermore, although still in their infancy, CL-based theragnostics could represent a relevant tool, solving the main problem of approaches heavily relying on external light, i.e. shallow tissue penetration of UV light, by exploiting CL reactions as an inner light source.

On the other hand, the detection of electrons combined with printed electronics has established electrochemical biosensors as the leading technology for the delivery of wearable sensors applied in biomedical field. To this regard, the huge attention in this research field during last years is due to the endearing features of these analytical tools, which encompasses the closeness of the point of care to the patients, the smart transmission data, the cost-effectiveness, and the on line monitoring of health parameters.

Hybrid amperometric and CL based biosensors could be developed taking advantages of the best analytical performance of the two principles, according to the expected analyte concentration and matrix complexity.

Moreover, the electrogenerated chemiluminescence (ECL) and biosensors based on this principle are very potent analytical tools in the portable area after the tremendous success of ECL in clinical chemistry analysed using Ruthenium complexes, (which releases a photon at ~620 nm) regenerating with excess of the co-reactant tripropylamine (Babarniri et al. 2019).

Therefore, we use an electrochemical process to trigger the light emission by generating a molecule its singlet excited state and we measure the photon emitted with a simple CCD or CMOS. Surprisingly ECL combines both electrons and photons in a different way but offers high potentiality in terms of simplicity and applicability in new generation of biosensors. Of course, the extraordinary detectability of ECL using the co-reactant derived from the cyclic amplification due to the excess of tripropylamine. Other ECL systems using for example luminol and platinum-gold alloy hybrid functionalized zinc oxide nanocomposites present similar analytical performance of the CL Systems (Huang et al., 2018a).

In conclusion, electrochemisty and CL based biosensors offer similar performance in terms of sensitivity that are superior to other transduction principles such as for example optical and photoluminescence.

Differences among them often reported are related mainly to the optimization of the assay conditions, reagents used and analytical procedure.

7. REFERENCES

Abbaspour, A., Norouz-Sarvestani, F., Noori, A., Soltani N., 2015. Biosens. Bioelectron. 68, 149-155.

Albrecht, HO., 1928. Chemical. 136, 321–330.

Ambrosi, A., Chua, C.K., Khezri, B., Sofer, Z., Webster, R.D., Pumera, M., 2012a. Proc. Natl. Acad. Sci. 109, 12899-12904.

Ambrosi, A., Chee, S.Y., Khezri, B., Webster, R.D., Sofer, Z., Pumera, M., 2012b. Angew. Chem., Int. 51, 500-503.

Ambrosi, A., Chua, C.K., Bonanni, A., Pumera, M., 2014. Chem. Rev. 114, 7150-7188.

Andronico, L.A., Chen, L., Mirasoli, M., Guardigli, M., Quintavalla, A., Lombardo, M., Trombini, C., Chiu, D.T., Roda, A., 2018. Nanoscale 10(29), 14012-14021.

Arduini, F., Cinti, S., Caratelli, V., Amendola, V., 2019. Biosens. Bioelectron. 126, 346-354.

Arduini, F., Neagu, D., Dall'Oglio, S., Moscone, D., Palleschi, G., 2012a. Electroanalysis. 24(3), 581-590.

Arduini, F., Di Nardo, F., Amine, A., Micheli, L., Palleschi, G., Moscone, D., 2012b. Electroanalysis. 24(4),743-751.

Babarniri, B., Bahari, D., Salimi, A., 2019. Biosens. Bioelectron. 142, 111530.

Bonanni, A., Chua, C. K., Zhao, G., Sofer, Z., Pumera, M., 2012. ACS nano. 6(10), 8546-8551.

Campbell, R.L., Wagner, D.B., O'Connel, J.P., 1987 Solid-phase assay with visual readout, US Pat. 4,703,017

Choudry, N. A., Kampouris, D. K., Kadara, R. O., & Banks, C. E., 2010. Electrochem. Commun. 12(1), 6-9.

Cinti, S., Arduini, F., Vellucci, G., Cacciotti, I., Nanni, F., & Moscone, D., 2014. Electrochem. Commun. 47, 63-66.

Cinti, S., Neagu, D., Carbone, M., Cacciotti, I., Moscone, D., 2016a. Electrochim. Acta. 188, 574-581

Cinti, S., Talarico, D., Palleschi, G., Moscone, D., Arduini, F., 2016b. Anal. Chim. Acta. 919, 78-84.

Cinti, S., Arduini, F., 2017. Biosens. Bioelectron. 89, 107-122.

Cinti, S., Minotti, C., Moscone, D., Palleschi, G., Arduini, F. 2017. Biosens. Bioelectron. 93, 46-51.

Cinti, S., Proietti, E., Casotto, F., Moscone, D., & Arduini, F. 2018. Anal. Chem. 90(22), 13680-13686.

Cinti, S., Moscone, D., Arduini, F., 2019. *Nature protocols*, *14*(8), 2437-2451.

Cui, G., Yoo, J.H., Lee, J.S., Yoo, J., Uhm, J.H., Cha, G.S., Nam, H., 2001. Analyst. 126, 1399-1403.

Di Fusco, M., Quintavalla, A., Lombardo, M., Guardigli, M., Mirasoli, M., Trombini, C., Roda, A., 2015. Anal. Bioanal. Chem. 407, 1567–1576

Du, D., Wang, L., Shao, Y., Wang, J., Engelhard, M. H., & Lin, Y., 2011. *Anal. Chem.* 83, 746-752.

Dungchai, W., Chailapakul, O., Henry, C. S., 2009. *Anal. Chem. 81*(14), 5821-5826.

Escarpa A., 2012. Chem. Rec. 12, 72-91. Fanjul-Bolado, P., Hernández-Santos, D., José Lamas-Ardisana, P., Martín-Pernía, A., Costa-García, A., 2008. Electrochim. Acta. 53, 3635-3642.

Ghamouss, F., Tessier, P.Y., Djouadi, M.A., Besland, M.P., Boujtita, M., 2007. Electrochem. Commun. 9(7), 1798-1804.

Goh, M.S., Pumera, M., 2010. Anal. Chem. 82, 8367-8370.

Guan, W.J., Li, Y., Chen, Y.Q., Zhang, X.B., Hu, G.Q., 2005. Biosens. Bioelectron. 21, 508-512.

Hananya, N., Eldar Boock, A., Bauer, C.R., Satchi-Fainaro, R., Shabat, D., 2016. J. Am. Chem. Soc. 138, 13438−13446

Huang, X., Deng, X., Qi, W., Wu, D., 2018a. Sens. Actuat. B-Chem. 273, 466-472

Huang, Y., Gao, L., Cui, H., 2018b. ACS Appl. Mater. Interfaces. 10 (20), 17040-17046.

Iinuma, M., Kadoya, Y., Kuroda, A. 2016. Methods Mol Biol. 1461, 299-310.

Im, J.H., Kim, H.R., An, B.G., Chang, Y.W., Kang, M.J., Lee, T.G., Son, J.G., Park, J.G., Pyun, J.C., 2017. Biosens. Bioelectron. 92, 221-228.

Inzelt, G., Lewenstam, A., Scholz, F., 2013. Handbook of reference electrodes. Springer.

Ives, D.J., Janz, G.J., 1961. Reference Electrodes, Academic Press, New York, p. 179.

Kadara, R. O., Jenkinson, N., Banks, C. E., 2009. Electrochem. Commun. 11, 1377–1380.

Kampouris D.K., Banks C.E., 2010. Chem. Commun. 46, 8986-8988.

Li, F. Liu, JC. Guo, L. Wang, JH. Zhang, KQ. He, JB. Cui, H., 2019. Biosens. Bioelectron. 141, 111472.

Li, N., Liu, D., Cui, H., 2014. Anal. Bioanal. Chem. 406(23), 5561-5571.

Li, X., Liu, B., Hun, X., 2018. Sens. Actuator B-Chem. 277, 510–516.

Lin, Y., Lu, F., Wang, J., 2004. Electroanalysis 16, 145-149.

Ling, P., Lei, J., Jia, L., & Ju, H., 2016. Chem. Commun. 52(6), 1226-1229.

Ma, T., Zhang, M., Wan, Y., Cui, Y., Ma, L., 2017. Micromachines 8(5), 149

Marzocchi, E., Grilli, S., Della Ciana, L., Prodi, L., Mirasoli, M., Roda, A., 2008. Anal. Biochem. 377(2), 189-194.

Mazzaracchio, V., Neagu, D., Porchetta, Al., Marcoccio, E., Pomponi, A., Faggioni, G., D'Amore, N., Notargiacomo, A., Pea, M., Moscone, D., Palleschi, G., Lista, F., Arduini, F., 2019. Biosens. Bioelectron. 126, 640-646.

Mirasoli, M., Bonvicini, F., Lovecchio, N., Petrucci, G., Zangheri, M., Calabria, D., Costantini, F., Roda, A., Gallinella, G., Caputo, D., de Cesare, G., Nascetti, A., 2018. Sens. Actuat. B-Chem. 262, 1024-1033.

Mirasoli, M., Guardigli, M., Michelini, E., Roda, A., 2014a. J. Phar. Biomed. Anal. 87, 36-52.

Mirasoli, M., Nascetti, A., Caputo, D., Zangheri, M., Scipinotti, R., Cevenini, L., de Cesare, G., Roda, A., 2014b. Anal. Bioanal. Chem. 406, 5645-5656.

Moscone D., D'Ottavi, D., Compagnone, D., Palleschi, G., Amine, A., 2001. Anal. Chem. 73, 2529-2535.

Morrin, A., Killard, J., Smyth, M.R., 2003. Anal. Lett. 36, 2021-2039.

Nakazono, M., Oshikawa, Y., Nakamura, M., Kubota, H., Nanbu, S., 2017. J. Org. Chem. 82(5), 2450-2461

Nascetti, A., Mirasoli, M., Marchegiani, E., Zangheri, M., Costantini, F., Porchetta, A., Iannascoli, L., Lovecchio, N., Caputo, D., de Cesare, G., Pirrotta, S., Roda, A., 2019. Biosens. Bioelectron. 123, 195-203.

Park, JM., Jung, HW., Chang, YW., Kim, HS., Kang, MJ., Pyun, JC., 2015. Anal. Chim. Acta. 853, 360-367.

Ping, J., Wang, Y., Fan, K., Wu, J., Ying, Y., 2011. Biosens. Bioelectron. 28, 204-209.

Rezazadeh, M., Seidi, S., Lid, M., Pedersen-Bjergaard, S., Yamini, Y., 2019. TrAC-trend. Anal. Chem. 118, 548-555.

Roda, A., Michelini, E., Caliceti, C., Guardigli, M., Mirasoli, M., Simoni, P., 2018. Anal. Bioanal. Chem. 410(3), 669-677.

Roda, A., Mirasoli, M., Dolci, L.S., Buragina, A., Bonvicini, F., Simoni, P., Guardigli, M., 2011. Anal. Chem. 83, 3178-3185.

Roda, A., Mirasoli, M., Michelini, E., Di Fusco, M., Zangheri, M., Cevenini, L., Roda, B., Simoni, P., 2016. Biosens. Bioelectron. 76, 164-179.

Roda, A., Zangheri, M., Calabria, D., Mirasoli, M., Caliceti, C., Quintavalla, A., Lombardo, M., Trombini, C., Simoni, P., 2019. Sens. Actuator B-Chem. 279, 327-333.

Sakharov, I.Y., Vdovenko, M.M., 2013. Anal. Biochem. 434, 12–14

Scordo, G., Moscone, D., Palleschi, G., Arduini, F., 2018. Sens. Actuator. B-Chem. 258, 1015-1021.

Setford, S.J., Van Es, R.M., Blankwater, Y.J., Kröger, S., 1999. Anal. Chim. Acta. 398, 13–22.

Schaap, A.P., Handley, R.S., Giri, B.P., 1987. Tetrahedron Lett. 28, 935-938.

Shu, J., Han, Z., Cui, H., 2019. Anal. Bioanal. Chem. 411, (18) 4175-4183.

Singh S., Jain D.V.S., Singla M.L., 2013. Sens. Actuat. B. 182 161-169.

Soares, RRG., Santos, D.R., Chu, V., Azevedo, A.M., Aires-Barros, M.R., Conde, J.P., 2017. Biosens. Bioelectron. 87, 823-831.

Tang S., Tong, P., Lu, W., Chen, J., Yan, Z., Zhang, L., 2014. Biosens. Bioelectron. 15 (59), 1-5.

Tiwari A., Dhoble S.J., 2018. Talanta. 180, 1-11.

Wang, D.M., Lin, K.L., Huang, K.Z., 2019. Luminescence. 34, 4–22.

Wang, J., Musameh, M., 2004. Analyst 129 (1), 1-2.

Wang, J., Pedrero, M., Sakslund, H., Hammerich, O., Pingar-ron, J., 1996. Analyst, 121, 345-350.

Wang, J., Tian, B., Nascimento, V. B., Angnes, L., 1998. Electrochim. Acta. 43, 3459–3465.

Wang, J., Zhong, WH., Liu, X.Y., Yang, T.T., Li, F., Li, Q., Cheng, W.R., Gao, C., Jiang, Z., Jiang, J., Cui, H., 2017. Anal. Chem. 89, (24) 13518-13523.

Wang, T., Randviir, E. P., Banks, C. E., 2014. *Analyst*. 139, 2000–2003.

Wei, H., Sun, J.J., Xie, Y., Lin, C.G., Wang, Y.M., Yin, W.H., Chen, G.N., 2007. Anal. Chim. Acta. 588, 297-303.

Yoon, Y.J., Li, K.H.H., Low, Y.Z., Yoon, J., Ng, S.H., 2014. Sens. Actuator B-Chem. 198, 233-238

Zangheri, M., Cevenini, L., Anfossi, L., Baggiani, C., Simoni, P., Di Nardo, F., Roda, A. 2015. Biosens. Bioelectron. 64, 63-68.

Zangheri, M., Di Nardo, F., Anfossi, L., Giovannoli, C., Baggiani, C., Roda, A., Mirasoli, M., 2015. Analyst 140(1), 358-365.

Zangheri, M., Di Nardo, F., Mirasoli, M., Anfossi, L., Nascetti, A., Caputo, D., De Cesare, G., Guardigli, M., Baggiani, C., Roda, A. 2016. Anal. Bioanal. Chem. 408, 8869-8879.

Zangheri, M., Mirasoli, M., Guardigli, M., Di Nardo, F., Anfossi, L., Baggiani, C., Simoni, P., Benassai, M., Roda, A., 2019. Biosens. Bioelectron. 129, 260-268.

Zhang, Z.F., Cui, H., Lai, C.Z., Liu, L.J., 2005. Anal. Chem. 77, 3324-3329.

Zhang, H., Liu, M., Huang, G., Yu, Y., Shen, W., Cui, H., 2013. J. Mater. Chem. B, 1, 970-977.

Zhu, N., Gu, L., Wang, J., Li, X., Liang, G., Zhou, J., Zhang, Z., 2019a. J. Phys. Chem. C 123, 9388-9393.

Zhu, G.Y., Yin, X.D., Jin, D.L., Zhang, B., Gu, Y.Y., An, Y.R., 2019b. TrAC-trend. Anal. Chem. 111, 100-117.

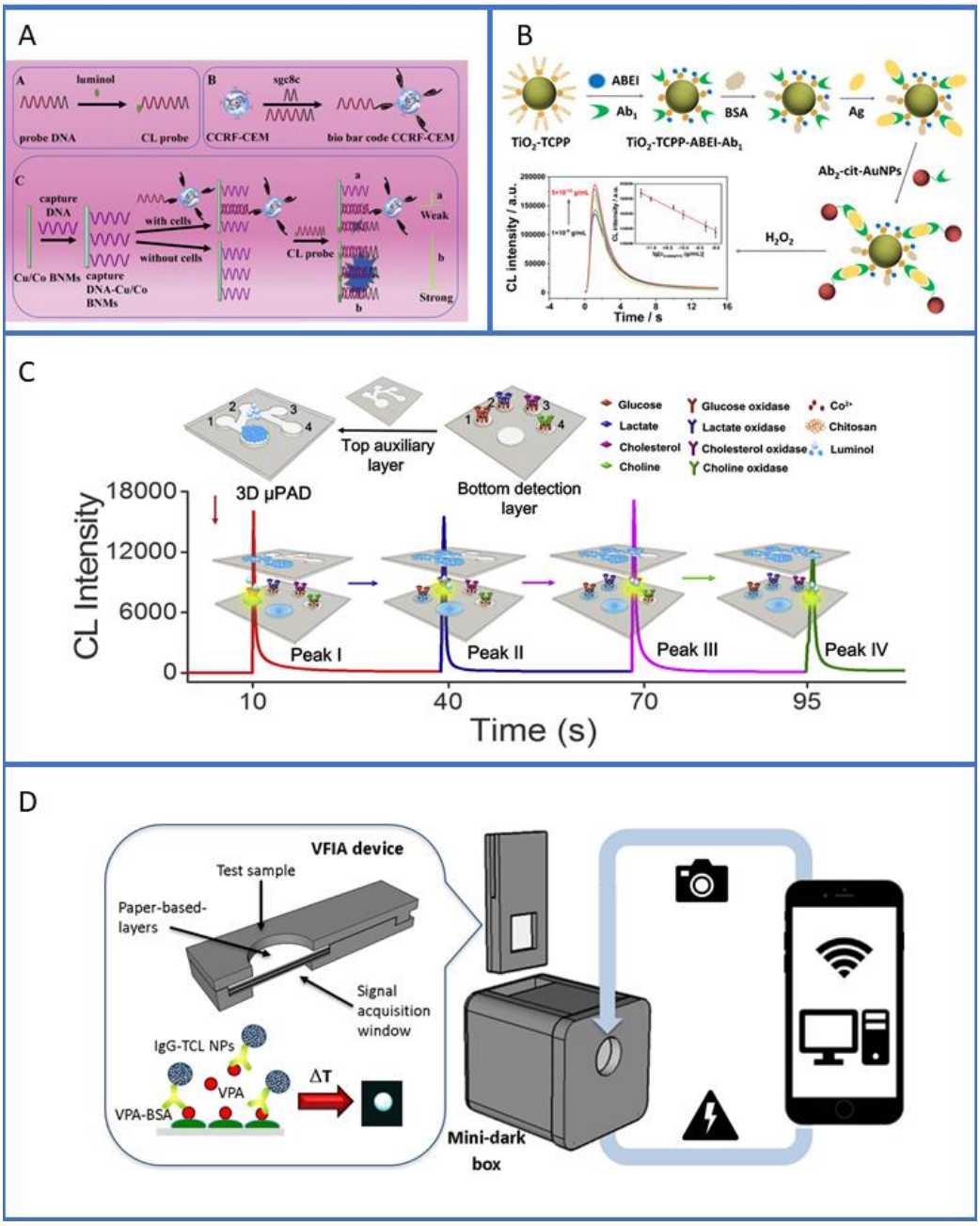

Figure 1. Examples of different strategies for improving luminescence quantum yield and innovative CL-based analytical formats. A) Cu/Co bimetallic manomaterials, employed as the nanocatalysts for the CL reaction, enabling detection of cancer cells down to 270 cells mL^{-1} in an aptamer-based assay (Li et al., 2018); B) Turn-off CRET-based sandwich immunoassay exploiting TiO_2 NPs functionalized with a porphyrin derivative and N-(4-aminobutyl)-N-ethylisoluminol (TiO_2-TCPP-ABEI nanoluminophores) as CL emitter and AuNPs as energy acceptor (Shu et al., 2019); C) a double-layered three-dimensional (3D) microfluidic network was exploited for temporizing reagents delivery, thus developing a multiplex CL enzyme assay for detecting glucose, lactate, choline, and cholesterol (Li et al., 2019); D) Smartphone-based thermochemiluminescent immunosensor for valproic acid detection (Roda et al., 2019).

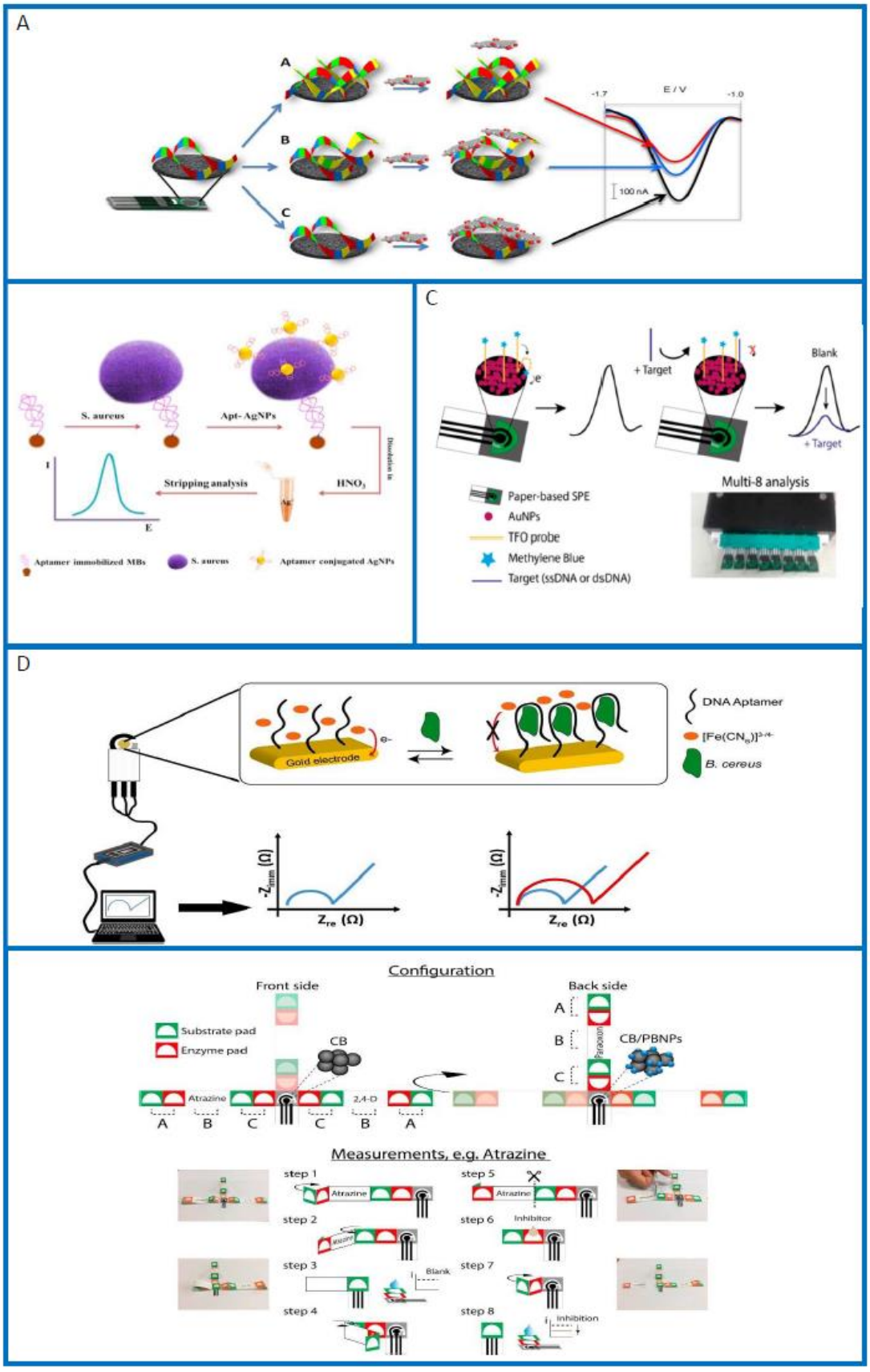

Figure 2. Examples of different cutting-edge technologies used for the development of miniaturised and smart electrochemical biosensors. A) Exploitation of inherently electroactive graphene oxide

nanoplatelets for the detection of single-nucleotide polymorphism by following the interactions between graphene oxide nanoplatelets and DNA strands (Bonanni et al., 2012). B) Aptamer and silver nanoparticles combined with magnetic beads for electrochemical determination of *S. aureus* (Cinti et al., 2018). C) Sensor arrays for the detection of single and double stranded DNA targets using a multi-8 reader (Cinti et al., 2018) D) Portable potentiostat and gold screen-printed electrode modified with selected aptamer for *B. anthracis* spore simulant (*B. cereus)* detection (Mazzaracchio et al., 2019). E) An origami paper-based device for a fast and cost-effective multianalysis of several classes of pesticides (Arduini et al., 2019).

Figure 3. Layout of experimental protocols employed for biosensing measurements in this work.

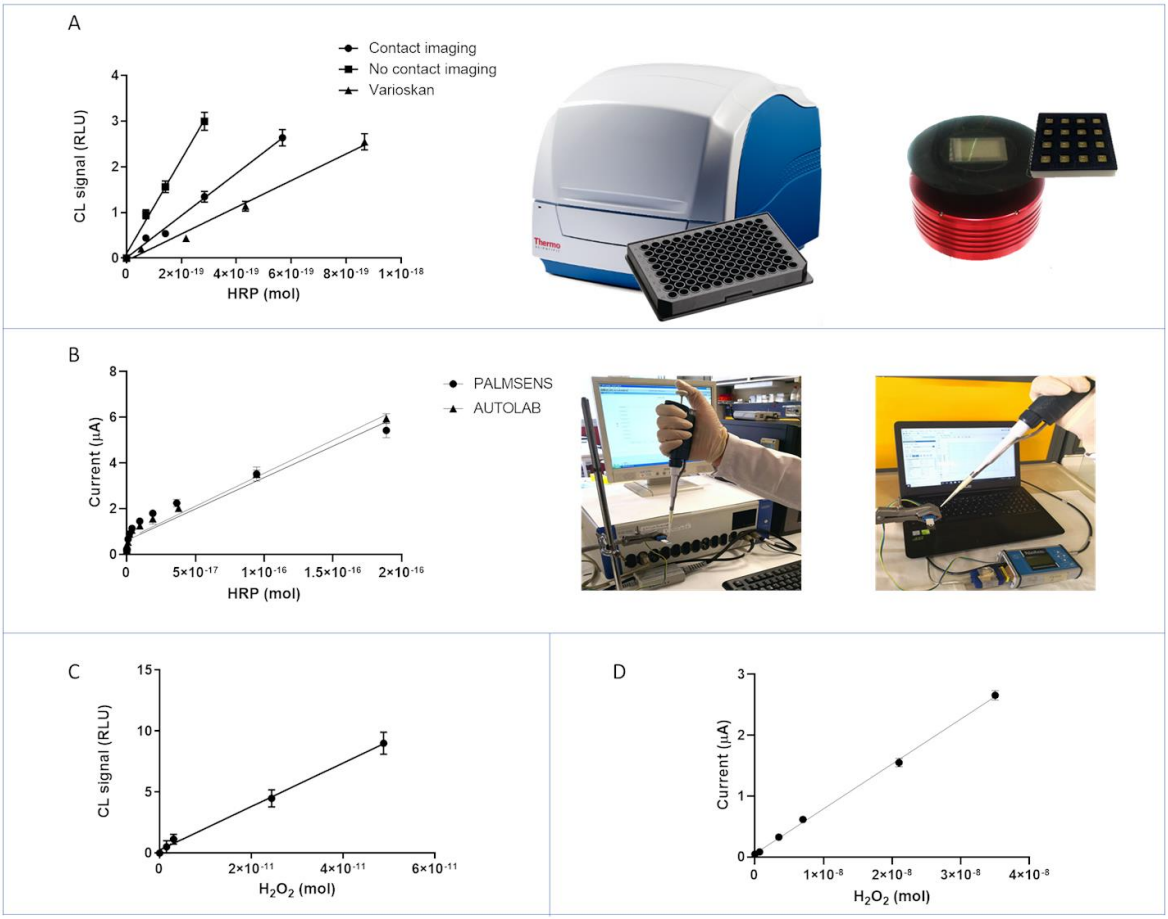

Figure 4. A) Calibration curve of HRP by CL-based detection, employing the Varioskan bench-top instrumentation (triangles) or the cooled CCD-based portable device employed in the contact (circle) or optics-based (squares) configuration. B) Calibration curve of HRP using electrochemical sensor based on SPE modified with CB and portable instrument (blue line) or laboratory benchtop instrumentation (black line). C) CL calibration curve of H_2O_2 using laboratory benchtop Varioskan instrumentation. D) Calibration curve of H_2O_2 using laboratory benchtop instrumentation and SPE modified with CB/PBNPs.

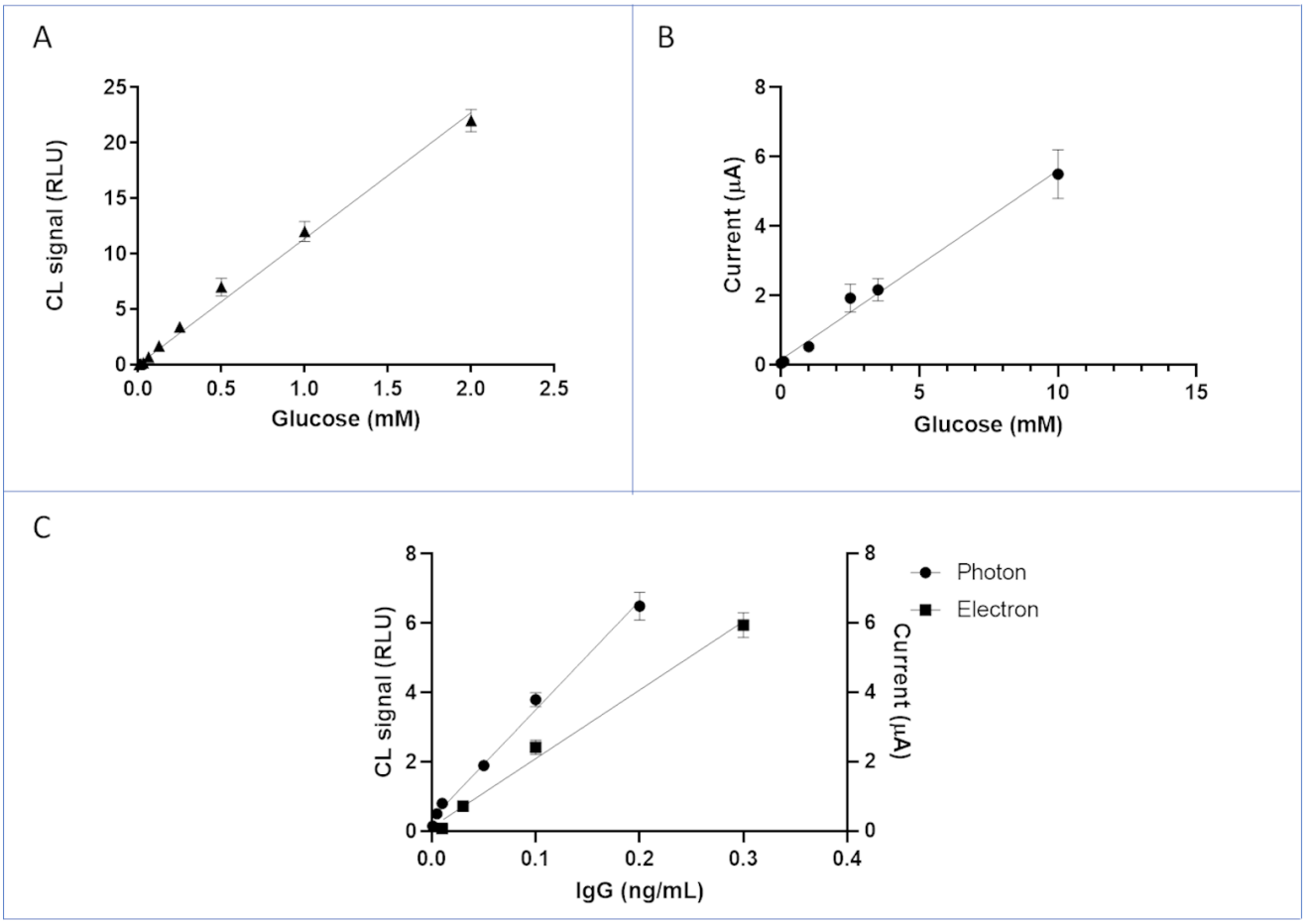

Figure 5. A) Calibration curve for glucose by CL detection employing a paper-based GOx sensor and portable CCD-based instrumentation. B) Calibration curve of glucose using SPE printed on office paper and modified with CB/PBNPs combined with filter paper pad and portable instrument. C) IgG measurement by using a sandwich immunoassay with magnetic beads and CL detection D) IgG measurement by using a sandwich immunoassay with magnetic beads and SPE modified with CB.

Table 1. Analytical performances of selected recently reported CL and electrochemical biosensors

Analyte	Biosensing principle	Detection	Analytical features	Reference
CL-based biosensors				
Organic compounds containing hydroxyl (OH), amino (NH_2), or mercapto (SH) groups.	Analytes interact with gold nanoparticles leading to a change in CL intensity.	Laboratory-built flow injection CL system.	LOD: 10^{-10} mol L^{-1} Linear range: 3 orders of magnitude.	Zhang et al., 2005
Human IgG and other proteins.	Label-free immunoassay based on multifunctionalized gold nanoparticles (MF-GNPs), obtained by successive assembly of ABEI-GNPs with antibody, bovine serum albumin (BSA) and Co^{2+}.	Microplate luminometer.	LOD: 0.13 fmol L^{-1} Dynamic range: 1.0 fmol L^{-1} to 1.0 nmol L^{-1}.	Huang et al., 2018
Cancer cells.	Aptamer-based assay employing Cu/Co bimetallic manomaterials with enhanced catalytical ability as nanocatalysts for the CL reaction.	Flow injection CL system equipped with a photomultiplier.	LOD: 270 cells mL^{-1}	Li et al., 2018
Copeptin, a surrogate marker for acute myocardial infarction.	Turn-off CRET-based sandwich immunoassay exploiting TiO_2 NPs functionalized with a porphyrin derivative and N-(4-aminobutyl)-N-ethylisoluminol and AuNPs as the CL emitter and energy acceptor, respectively.	Microplate luminometer.	LOD: 1.54×10^{-12} g mL^{-1}. Dynamic range: 5×10^{-12} - 1×10^{-9} g mL^{-1}	Shu et al., 2019
Glucose in human urine	2D-MOF nanosheet with peroxidase activity functionalized with luminol and glucose oxidase (GOD), to yield a Co-TCPP(Fe)@luminol@GOD composite material able to generate a CL signal upon simple addition of the sample.	Not reported	LOD: 10.667 µg L^{-1}. Dynamic range: 32–5500 µg L^{-1}	Zhu et al., 2019a
Parvovirus B19 DNA	Solid-phase DNA hybridization reaction performed in a transparent microfluidic device, followed by antibody-HRP-based CL detection.	Lensless contact imaging on a ultrasensitive cooled charge-coupled device (CCD) camera.	LOD: 0.05 µmol L^{-1}, corresponding to 50 fmol of DNA amplification product.	Roda et al., 2011
Cortisol in saliva	Lateral flow immunoassay (LFIA) with CL detection, performed in a 3D-printed cartridge containing a sealed fluidic element.	Lensless contact imaging on a ultrasensitive cooled charge-coupled device (CCD) camera.	LOD: 0.2 ng mL^{-1}	Zangheri et al., 2019

Valproic acid in blood and saliva.	One-step competitive vertical flow immunoassay (VFIA), employing silica nanoparticles doped with a thermochemiluminescent (TCL) 1,2-dioxetane derivative as a label.	By 3D printing, simple accessories were produced to turn a smartphone into a biosensing device that provides a power source for the heat shock required to trigger the TCL reaction and a sensitive camera for measuring emitted photons.	Blood: LOD 4 μg mL^{-1}; Dynamic range 4–300 μg mL^{-1}. Saliva: LOD 0.05 μg mL^{-1}; Dynamic range 0.05–20 μg mL^{-1}	Roda et al., 2019
Ochratoxin A (OTA), aflatoxin B1 (AFB1) and deoxynivalenol (DON) in food and feedstock.	Microfluidic multiplexing methodology based on the concept of micromosaic immunoassays for mycotoxins immunodetection.	Microfabricated a-Si:H photoconductors.	LOD: 0.1, 0.3 and 1 ng mL^{-1} for AFB1, DON and OTA, respectively.	Soares et al., 2017
Carcinoembryonic antigen.	ELISA kit based on CL immunoassay.	Miniaturized photosensor obtained by *in situ* synthesis of cadmium sulphide nanowires on the gold surface of an interdigitated electrode.	LOD: 3.2 ng mL^{-1}	Im et al., 2017
Glucose, lactate, cholesterol, choline.	Multiplex CL enzyme assay performed on a double-layered three-dimensional (3D) microfluidic network, exploited for temporizing reagents delivery	Photomultiplier tube.	LOD: glucose 8 μmol L^{-1}, lactate 15 μmol L^{-1}, choline 6 μmol L^{-1}, and cholesterol 0.07 μmol L^{-1}. Dynamic ranges: glucose 0.01–1.0 mmol L^{-1}, lactate 0.02–5.0 mmol L^{-1}, cholesterol 0.01–0.4 mmol L^{-1}, and choline 0.001–1.0 mmol L^{-1}.	Li et al., 2019
Human chorionic gonadotropin (hCG).	CL LFIA employing Pt NPs with catalytic activity as enzyme-mimic label.	Ultrasensitive CCD-based imaging.	LOD: 1 mIU mL^{-1}	Park et al., 2015
IgG	TCL semiconducting polymer dots (TCL-Pdots) as luminescent nanolabels for immunobiosensors.	TCL signal was acquired through a portable CCD camera.	LOD: 13 nmol L^{-1} Dynamic range: up to 230 nmol L^{-1}	Andronico et al., 2018

Electrochemical biosensors				
Glucose.	Electrochemical biosensing platform using electrochemically reduced graphene oxide (ER-GNO) and ionic liquid doped screen-printed electrode (ER-GNO/IL-SPE) modified with glucose oxidase electrode.	CHI 440 electrochemical workstation.	LOD: 1.0 μM Linear range: 5 - 12 mM.	Ping et al., 2011
Phosphorylated p53 (S392).	Electrochemical immunosensor for ultrasensitive detection of phosphorylated p53 at Ser392 (phospho-$p53^{392}$) based on graphene oxide (GO) as a nanocarrier in a multienzyme amplification strategy.	CHI 440 electrochemical workstation.	LOD: 0.01 nM Linear range: 0.02 - 2 nM.	Du et al., 2011
Single nucleotide polymorphism.	Graphene oxide nanoplatelets (GONPs) as electroactive labels for DNA analysis.	Autolab PGSTAT302 potentiostat.	The e limit of detection was 500 pM. The differentiation between the wild-type and mutant was detectable at 10 nM.	Bonanni et al., 2012
Catechol.	Sol–gel based composite of polivinilpirrolidone (PVP) stabilized gold nanoparticles as matrix for tyrosinase in an amperometric biosensor.	CHI-Instruments Model 660.	LOD: 0.3 μM. Linear range: 1.0 - 6 μM.	Singh et al., 2013
Hg(2+).	Label-free electrochemical sensor based on the catalytic formation of Au nanoparticle accelerated by Hg^{2+} and detected by stripping voltammetry.	CHI760D electrochemical analytical system.	LOD: 0.06 nM. Linear range: 0.5 - 120 nM.	Tang et al., 2014
S. aureus.	Aptamer-conjugated silver nanoparticles for electrochemical dual-aptamer-based sandwich bioassay.	μAutolab type III.	LOD: 1 CFU mL^{-1}. Dynamic range: 10 - 10^6 CFU mL^{-1}.	Abbaspour et al., 2015
Telomerase activity in cell.	Platinum nanoparticles encapsulated in metal–organic frameworks (MOFs) used for telomerase activity evaluation following the Pt NP electrocatalysis.	CHI 660D electrochemical workstation.	LOD: 1 x 10^2 cells mL^{-1}. Dynamic range: 5 x 10^2 – 1 x 10^7 cells mL^{-1}. Activity calculated in a single cell: 2 × 10^{-11} IU.	Ling et al., 2016

(ssDNA) and (dsDNA).	Miniaturised Paper-based electrochemical sensor modified with gold nanoparticles utilizing triplex forming oligonucleotides (TFO) tagged with methylene blue (MB) as the recognizing probes.	Portable potentiostat PalmSens equipped with a multiplexer for 8 cells and connected to a laptop..	LOD: 3 and 7 nM, for (ssDNA) and (dsDNA) sequences, respectively.	Cinti et al., 2018
B. cereus spore.	Gold screen-printed electrode modified with DNA-based aptamer for an impedimetric label-free sensor.	Portable potentiostat PalmSens[3].	LOD: 3×10^3 CFU mL^{-1}. Linear range: 10^4 - 5×10^6 CFU mL^{-1}.	Mazzaracchio et al., 2019
Organophosphorus pesticide.	A graphite screen-printed electrode modified with carbon black-cobalt phthalocyanine nanocomposite and immobilized Butyrylcholinesterase enzyme.	Portable potentiostat PalmSens.	LOD: 18 nm. Linear range up to 110 nM.	Cinti et al., 2016a
Nerve agent.	Microfluidics biosensor chip with integrated screen-printed electrodes modified with acetylcholinesterase.	DY2000 Series Multi-Channel Potentiostat.	Not reported	Yoon et al., 2014
Nerve agent.	Screen-printed electrodes modified with butyrylcholinesterase integrated in microfluidic chip.	Portable potentiostat PalmSens.	LOD: 20 ppb. Linear range up to 60 ppb.	Arduini et al., 2012a
Glucose, lactate, and uric acid.	Coupling of electrochemical detection and paper microfluidics to provide rapid quantitative measurement of critical health markers in serum.	CHI 1207A potentiostat.	Glucose: LOD 0.21 mM, linear range 0-100 mM. Lactate: LOD 0.36 mM, linear range 0-50 mM. Uric acid: LOD 1.38 mM, linear range 0-35 mM.	Dungchai et al., 2009
Nerve agent.	Fully integrated ready-to-use paper-based electrochemical biosensor.	Portable potentiostat PalmSens.	LOD: 3 μgL^{-1}. Linear range up to 25 μgL^{-1}.	Cinti et al., 2017
Paraoxon, 2,4-dichlorophenoxyacetic acid, and atrazine.	3D paper-based origami reagentless device for electrochemical measurement of 3 pesticides.	Portable potentiostat PalmSens.	Paraoxon: LOD 2 ppb, linear range up to 20 ppb. 2,4-dichlorophenoxyacetic acid: LOD 50 ppb, linear range up to 600 ppb Atrazine: LOD ppb, linear range 10 – 100 ppb.	Arduini et al., 2019
Butyrylcholinesterase.	A reagent-free paper-based printed sensor embedded in a 3D printing device.	Portable EmStat Instrument.	LOD: 0.5 IU mL^{-1}. Linear range up to 12 IU	Scordo et al., 2018

			mL^{-1}.	

Table 2. Analytical performances of CL and electrochemical sensing tools

LOD	LOQ	Dynamic range	Assay time	LOD	LOQ	Dynamic range	Assay time
CL H_2O_2 measurements				**EC H_2O_2 measurements**			
1 x 10^{-7} mol L^{-1} (4 x 10^{-12} mol/well)	4 x 10^{-7} mol L^{-1} (1.6 x 10^{-11} mol/well)	up to 1,25 x 10^{-3} mol L^{-1} (5 x 10^{-8} mol/well)	No incubation time. Measurement time: 1s (Varioskan Flash Reader); 120s (CCD camera).	3 x 10^{-6} mol L^{-1} (2.1 x 10^{-10} mol/well)	7 x 10^{-6} mol L^{-1} (5.0 x 10^{-10} mol/well)	up to 5 x 10^{-4} mol L^{-1} (3.5 x 10^{-8} mol/well)	No incubation time. Measurement time: 60 s, using bench-top (Autlab) instrument.
CL HRP MEASUREMENTS				**EC HRP MEASUREMENTS**			
2 x 10^{-15} mol L^{-1} (4.5 x 10^{-20} mol/well)	9 x 10^{-15} mol L^{-1} (2.0 x 10^{-19} mol/well)	up to 1 x 10^{-9} mol L^{-1} (3 x 10^{-14} mol/well)	No incubation time. Measurement time: 1s (Varioskan Flash Reader); 120s (CCD camera).	2 x 10^{-15} mol L^{-1} (2.0 x 10^{-20} mol/well)	3,5 x 10^{-15} mol L^{-1} (3.5 x 10^{-20} mol/well)	up to 1.9 x 10^{-11} mol L^{-1} (1.9 x 10^{-16} mol(well)	10 min as incubation time. Measurement time: 60 s, using both bench-top (Autlab) and portable (Palm Sens) instruments.
CL GLUCOSE MEASUREMENTS				**EC GLUCOSE MEASUREMENTS**			
1.7 x 10^{-5} mol L^{-1}	2.3 x 10^{-5} mol L^{-1}	2x10^{-3} mol L^{-1}	No incubation time. Measurement time: 120s	4 x 10^{-5} mol L^{-1}	1.3 x 10^{-4} mol L^{-1}	1 x 10^{-2} mol L^{-1}	No incubation time. Measurement time: 300 s,

			(CCD camera).				using portable (Palm Sens) instrument.
CL IgG MEASUREMENTS				**EC IgG MEASUREMENTS**			
1.2 x 10^{-14} mol L^{-1}	1.6 x 10^{-13} mol L^{-1}	up to 1.3 x 10^{-12} mol L^{-1}	Incubation time: 30 min. Measurement time: 1s (Varioskan Flash Reader); 120s (CCD camera).	1.2 x 10^{-13} mol L^{-1}	2.7 x 10^{-13} mol L^{-1}	up to 6.7 x 10^{-12} mol L^{-1}	No incubation time. Measurement time: 60 s, using portable (Palm Sens) instrument.